Article

Not peer-reviewed version

Synthesis and Preclinical Evaluation of Two Novel 68Ga-labeled Bispecific PSMA/FAP-targeted tracers with 2-Nal-containing PSMA-targeted Pharmacophore and Pyridine-based FAP-targeted Pharmacophore

Arsyangela Verena , Helen Merkens , Chao-Cheng Chen , Devon E. Chapple , Lei Wang , Shreya Bendre , Antonio A. W. L. Wong , François Bénard , Kuo-Shyan Lin *

Posted Date: 13 November 2023

doi: 10.20944/preprints202311.0769.v1

Keywords: Bispecific radiotracers; PSMA; FAP; PET/CT; Gallium-68; prostate cancer

Article

Synthesis and Preclinical Evaluation of Two Novel ^{68}Ga-Labeled Bispecific PSMA/FAP-Targeted Tracers with 2-Nal-Containing PSMA-Targeted Pharmacophore and Pyridine-Based FAP-Targeted Pharmacophore

Arsyangela Verena [1], Helen Merkens [1], Chao-Cheng Chen [1], Devon E. Chapple [1], Lei Wang [1], Shreya Bendre [1], Antonio A. W. L. Wong [1], François Bénard [1,2,3] and Kuo-Shyan Lin [1,2,3,*]

[1] Department of Molecular Oncology, BC Cancer Research Institute, Vancouver, BC V5Z1L3, Canada
[2] Department of Molecular Imaging and Therapy, BC Cancer, Vancouver, BC V5Z4E6, Canada
[3] Department of Radiology, University of British Columbia, Vancouver, BC V5Z1M9, Canada
* Correspondence: klin@bccrc.ca; +1-604-675-8208

Abstract: Some bispecific radiotracers have been developed to overcome the limitations of monospecific tracers and improve detection sensitivity for heterogeneous tumor lesions. Here we aim to synthesize two bispecific tracers targeting prostate-specific membrane antigen (PSMA) and fibroblast activation protein (FAP), which are key markers expressed in prostate cancer. A pyridine-based FAP-targeted ligand was synthesized through multi-step organic synthesis, and then connected to the 2-Nal-containing PSMA-targeted motif. K_i(PSMA) values of Ga-complexed bispecific ligands, Ga-AV01084 and Ga-AV01088, were 11.6 ± 3.25 and 28.7 ± 6.05 nM, respectively, and the IC_{50}(FAP) values of Ga-AV01084 and Ga-AV01088 were 10.9 ± 0.67 and 16.7 ± 1.53 nM, respectively. The uptake values for PSMA-expressing LNCaP tumor xenografts were 9.05 ± 1.54 and 8.85 ± 1.25 %ID/g for [^{68}Ga]Ga-AV010184 and [^{68}Ga]Ga-AV01088, respectively, which were lower than the monospecific PSMA-targeted tracer [^{68}Ga]Ga-PSMA-617 (16.7 ± 2.30 %ID/g). The uptake values for FAP-expressing HEK293T:hFAP tumor xenografts were 1.90 ± 0.41 and 1.20 ± 0.25 %ID/g for [^{68}Ga]Ga-AV01084 and [^{68}Ga]Ga-AV01088, respectively, which were also lower than the monospecific FAP-targeted tracer, [^{68}Ga]Ga-AV02070 (7.93 ± 1.88 %ID/g). Further investigations are needed to optimize the selection of linkers and targeted pharmacophores to improve the tumor uptake of PSMA/FAP bispecific tracers for prostate cancer imaging.

Keywords: Bispecific radiotracers; PSMA; FAP; PET/CT; Gallium-68; prostate cancer

1. Introduction

Prostate cancer is the second most common cancer and the fifth leading cause of cancer death in men worldwide, with an estimation of 1,410,000 new cases and 375,304 deaths in 2020 [1]. Based on the recent cancer statistics by Siegel et al. [2], 5-year relative survival rates of localized and regional prostate cancer are > 99%, however it decreased significantly to 32% for metastatic prostate cancer patients. Therefore, early and accurate detection is important to further improve the survival rates of prostate cancer patients. Recently, the application of radiopharmaceuticals for non-invasive detection and treatment of prostate cancer has shown positive outcomes, such as improving positive-lesion detection rate and prolonging imaging-based progression-free survival [3,4]. One of the promising radiotracers for metastatic prostate cancer diagnosis, which has been approved by the US FDA, is [^{68}Ga]Ga-PSMA-11, that targets prostate-specific membrane antigen (PSMA) [5,6]. PSMA is a type II transmembrane glycoprotein, also known as folate hydrolase 1 and glutamate carboxypeptidase II [7,8], which has been shown to be overexpressed in prostate tumor and the neovasculature of other types of cancer, such as oral squamous cell, breast, and renal cancers [9–11]. Therefore, many attempts

 doi:10.20944/preprints202311.0769.v1

to develop PSMA-targeted radioligands for prostate cancer imaging and radioligand therapy have been made.

The clinical data from the PSMA-targeted radioligand therapeutic agent, [^{177}Lu]Lu-PSMA-617, were shown to be effective in treating metastatic castration-resistant prostate cancer (mCRPC) patients [3]. However, patients with low to no PSMA-expressing lesions are ineligible to benefit from this treatment [12,13]. This intra-patient heterogeneous PSMA expression in prostate cancer lesions can lead to worse overall survival due to PSMA-negative lesions being misdiagnosed as false-negative [14,15]. One strategy to improve lesion detection in this patient cohort is by using bispecific radioligands to target PSMA and other overexpressed proteins in prostate cancer lesions, such as fibroblast activation protein (FAP). FAP is a type II transmembrane serine protease [16] that is highly expressed by cancer-associated fibroblasts (CAFs) in the tumor microenvironment (TME) [17]. It is overexpressed in 90% of epithelial tumors, including prostate cancer [18,19], and its expression is associated with worse prognosis [20], making it a promising target for cancer diagnosis and therapy. In fact, many new promising FAP-targeted radioligands are being developed and some are being validated clinically, such as [^{68}Ga]Ga-FAPI-04 [21], [^{68}Ga]Ga-FAPI-46 [22], and [^{177}Lu]Lu-FAP-2286 [23]. Despite the potential of FAP-targeted radioligands shown in these studies, their tumor retention and efficacy have not been promising in the clinic. Hence, by targeting PSMA which is overexpressed in tumor and FAP which is overexpressed in the tumor stroma, we hypothesized that it would potentially increase the lesion detection rate and tumor retention in prostate cancer patients.

Previous studies have demonstrated the potential of utilizing bispecific radioligands to increase detection sensitivity of prostate cancer imaging, such as PSMA/gastrin-releasing peptide receptor (PSMA/GRPR) bispecific radioligands that have higher tumor uptake in PSMA- and GRPR-expressing mouse tumor models compared to the monospecific radiotracers [24]. Recently, several PSMA/FAP bispecific radioligands have been reported: ^{64}Cu-, ^{18}F, and ^{68}Ga-labeled PSMA/FAP bispecific radiotracers by Boinapally et al. [25], Hu et al. [26], and Wang et al. [27], respectively. Their studies confirmed the potential usage of PSMA/FAP bispecific ligands to improve tumor uptake in PSMA- and FAP-expressing tumor models in comparison to the monospecific counterparts.

Recently, our group also developed three ^{68}Ga-labeled bispecific PSMA/FAP radiotracers which incorporate quinoline-based FAP pharmacophore and anthracene-containing PSMA pharmacophore [28]. We observed a high blood uptake (5-12 %ID/g at 1 h post-injection) in the mouse model with decreased tumor uptake in comparison to the ^{68}Ga-labeled monospecific counterparts, PSMA-targeted [^{68}Ga]Ga-HTK03041 and FAP-targeted [^{68}Ga]Ga-FAPI-04. We suspected that the longer blood retention could be caused by the increased lipophilicity of the ligands and potential interaction, such as π–π stacking between the quinoline ring and anthracene ring which hindered the binding of tracers to FAP and PSMA, leading to decreased tumor uptake. Our goal in this study is to solve these issues and improve the binding affinity and tumor uptake by replacing the pharmacophores with less lipophilic motifs, such as replacing Ala(9-Anth) in the PSMA-targeted pharmacophore with 2-Nal and replacing the quinoline motif in the FAP-targeted pharmacophore with a more hydrophilic pyridine.

Many potent pyridine-based FAP inhibitors (FAPIs) have been reported [29,30], however there are still few reports on the development of pyridine-based FAP-targeted tracers. Previously we synthesized and evaluated two novel ^{68}Ga-labeled pyridine-based FAP-targeted tracers, [^{68}Ga]Ga-AV02053 and [^{68}Ga]Ga-AV02070, and compared their binding affinity and tumor uptake to that of [^{68}Ga]Ga-FAPI-04 [31]. We discovered that although [^{68}Ga]Ga-FAPI-04 has higher binding affinity towards FAP and higher tumor uptake, both of our pyridine-based tracers have lower uptake in blood, muscle and bone, leading to much higher tumor-to-background contrast ratios. Our results suggest that pyridine-based FAPI is more hydrophilic than quinoline-based FAPI, and has potential to help reduce blood uptake. Furthermore, we found that Ga-AV02070 (Figure 1A), which has a carbonyl group at the para position to the pyridine nitrogen, has a better binding affinity to FAP and a higher tumor uptake compared to Ga-AV02053, which has the carbonyl group at the meta position to the pyridine nitrogen. Hence, the pharmacophore of AV02070 is a promising candidate for the design of FAP-targeted tracers.

Preprints (www.preprints.org) | NOT PEER-REVIEWED | Posted: 13 November 2023 doi:10.20944/preprints202311.0769.v1

In this paper, we report the design, synthesis, and evaluation of two bispecific PSMA/FAP-targeted radiotracers, [^{68}Ga]Ga-AV01084 and [^{68}Ga]Ga-AV01088 (Figure 1B). The PSMA binding motif of AV01084 and AV01088 was based on the 2-Nal-containing PSMA-targeted tracer, [^{68}Ga]Ga-PSMA-617 (Figure 1A) [32], and their FAP-targeted motif was derived from our pyridine-based FAP-targeted radiotracer, [^{68}Ga]Ga-AV02070 (Figure 1A). The difference between the two tracers is the position of DOTA chelator linked to the lysine, which is the ε-amino group in AV01084 and the α-amino group in AV01088. Their potential for prostate cancer imaging was evaluated by *in vitro* competition binding assay, PET imaging, and *ex vivo* biodistribution studies in preclinical PSMA-expressing LNCaP and FAP-expressing HEK293T:hFAP tumor models. The results were then compared with those of corresponding monospecific tracers, [^{68}Ga]Ga-PSMA-617 and [^{68}Ga]Ga-AV02070.

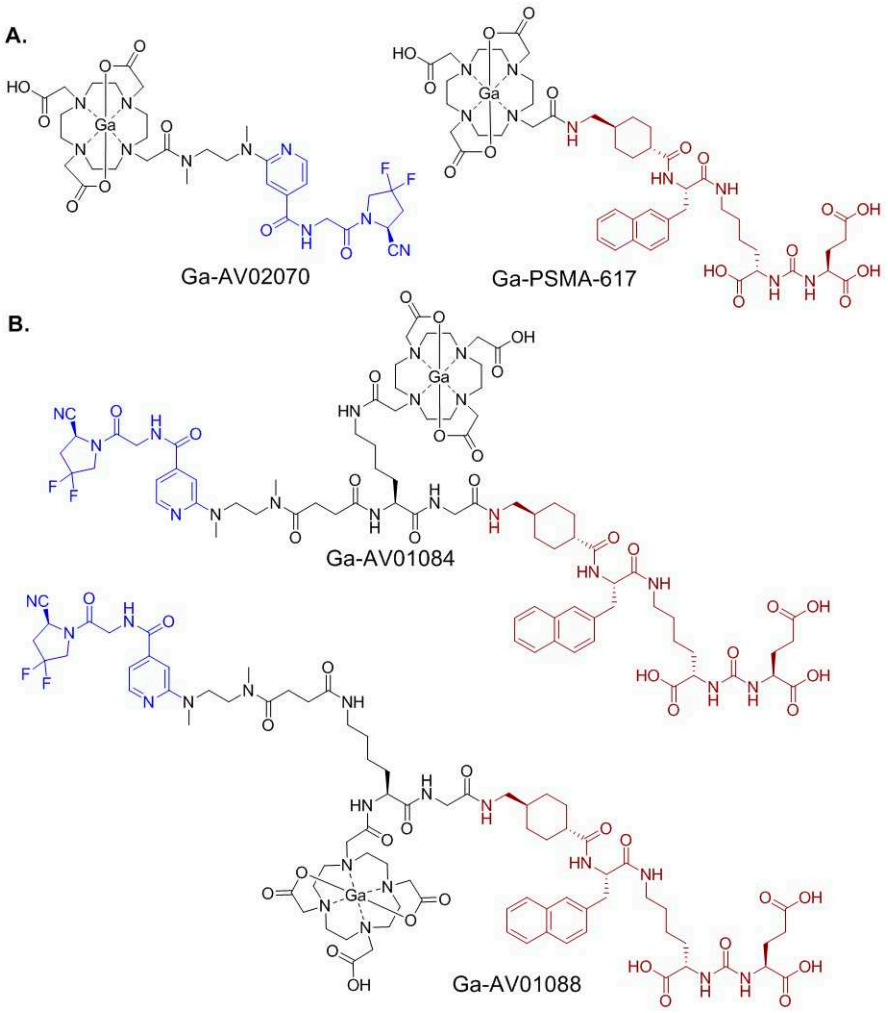

Figure 1. Chemical structures of (A) PSMA-targeted [^{68}Ga]Ga-PSMA-617 and FAP-targeted [^{68}Ga]Ga-AV02070; and (B) bispecific PSMA/FAP-targeted [^{68}Ga]Ga-AV01084 and [^{68}Ga]Ga-AV01088. The PSMA- and FAP-targeted pharmacophores are shown in brown and blue, respectively.

2. Results

2.1. Synthesis of PSMA/FAP Bispecific Ligand

AV01084 and AV01088 (Figure 1B) were synthesized on solid phase. Briefly, Lys(Lys(ivDde)-Gly-tranexamic acid-2-Nal)-urea-Glu(OtBu)-OtBu was first constructed on solid phase, followed by amide coupling of the FAP-targeted motif, compound **5**, and DOTA chelator. To synthesize compound **5** (Scheme 1), compound **1** was first coupled with 2,3,5,6-tetrafluorophenol (TFP) to obtain activated ester **2** in 71% yield. Compound **3** which was synthesized following literature procedures

Preprints (www.preprints.org) | NOT PEER-REVIEWED | Posted: 13 November 2023 doi:10.20944/preprints202311.0769.v1

[31] was first Boc-deprotected using trifluoroacetic acid (TFA), followed by coupling with compound **2** to obtain compound **4** in 45% yield. *t*-Butyl protecting group of compound **4** was removed using TFA and compound **5** was obtained quantitatively.

To synthesize AV01084, compound **5** was coupled to Lys(Lys(ivDde)-Gly-tranexamic acid-2-Nal)-urea-Glu(OtBu)-OtBu, followed by removal of the ivDde group at the Lys side chain and subsequent coupling with the DOTA chelator. To synthesize AV01088, DOTA chelator was first coupled to Lys(Lys(ivDde)-Gly-tranexamic acid-2-Nal)-urea-Glu(OtBu)-OtBu, followed by deprotection of amino group at the Lys side chain and coupling with compound **5**. The DOTA-conjugated ligands were then cleaved off from resin and purified by HPLC (Table S1). AV01084 and AV01088 were obtained in 12% and 7.2% yields, respectively.

Detailed syntheses and characterizations of nonradioactive Ga- and ^{68}Ga-complexed AV01084 and AV01088 are provided in the Supplementary Materials (Tables S2-S3). Nonradioactive Ga-complexed AV01084 and AV01088 were obtained in 60% and 21% yields, respectively, and their ^{68}Ga-labeled analogs were obtained in 33 – 64% decay-corrected radiochemical yields with ≥ 44 GBq/μmol molar activity and > 95% radiochemical purity.

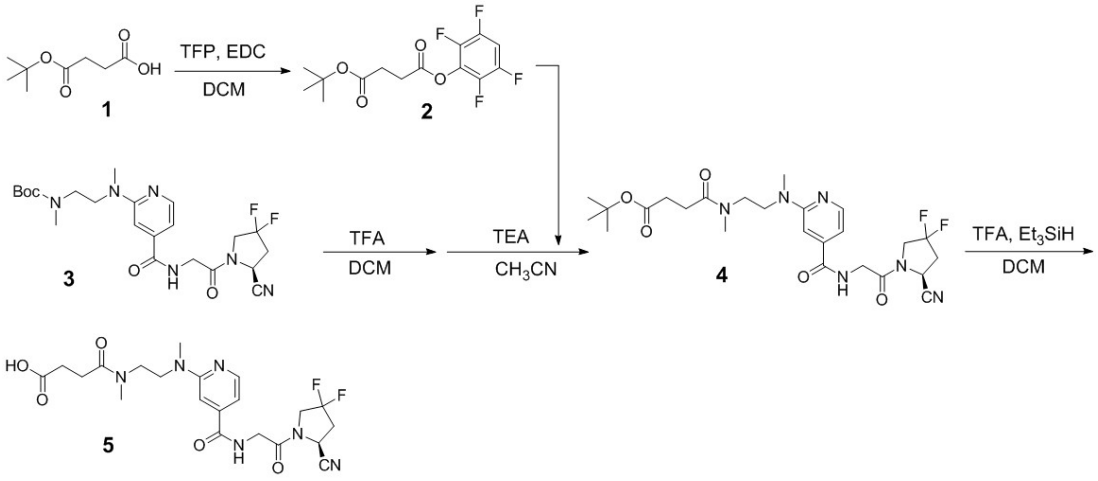

Scheme 1. Synthesis of (*S*)-4-((2-((4-((2-(2-cyano-4,4-difluoropyrrolidin-1-yl)-2-oxoethyl) carbamoyl)pyridin-2-yl)(methyl)amino)ethyl)(methyl)amino)-4-oxobutanoic acid (**5**).

2.2. Binding Affinity and Lipophilicity

The binding affinities of Ga-AV01084, Ga-AV01088, and Ga-AV02070 to PSMA were measured by a cell-based binding assay using PSMA-expressing LNCaP prostate cancer cells and were compared to the previously published Ga-PSMA-617 (K_i = 1.23 ± 0.08 nM) [33]. These ligands inhibited the binding of [^{18}F]DCFPyL to LNCaP cells in a dose-dependent manner (Figure 2A) and the calculated K_i(PSMA) values for Ga-AV01084, Ga-AV01088, and Ga-AV02070 were 11.6 ± 3.25, 28.7 ± 6.05, and > 1,000 nM, respectively (n = 3).

The binding affinities of Ga-AV01084, Ga-AV01088, and Ga-PSMA-617 to human FAP were measured by an enzyme inhibition assay using Suc-Gly-Pro-AMC as the FAP substrate and were compared to the previously published Ga-AV02070 (IC_{50} = 17.1 ± 4.6 nM) [31]. The human FAP enzymatic activity on the substrate was inhibited by these ligands in a dose dependent-manner (Figure 2B). The calculated IC_{50} values for Ga-AV01084, Ga-AV01088, and Ga-PSMA-617 were 10.9 ± 0.67, 16.7 ± 1.53 and > 1,000 nM respectively (n = 3).

Preprints (www.preprints.org) | NOT PEER-REVIEWED | Posted: 13 November 2023 doi:10.20944/preprints202311.0769.v1

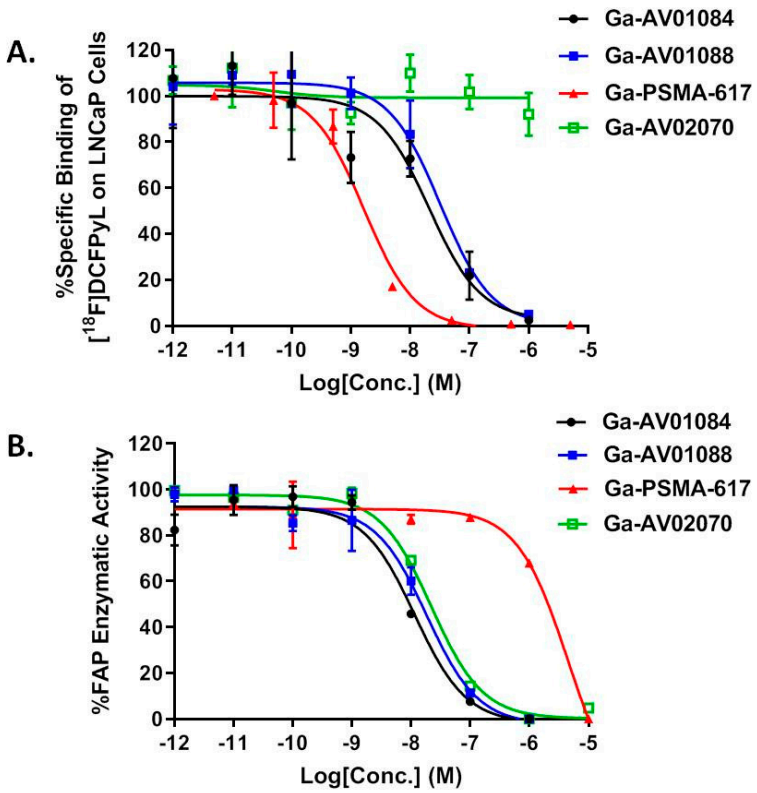

Figure 2. (A) Displacement curves of [^{18}F]DCFPyL by Ga-AV01084, Ga-AV01088, Ga-AV02070, and Ga-PSMA-617 generated using PSMA-expressing LNCaP cells; (B) Fluorescence curve of FAP enzymatic activity on Suc-Gly-Pro-AMC substrate with inhibition by Ga-AV01084, Ga-AV01088, Ga-AV02070, and Ga-PSMA-617.

The lipophilicity of the ^{68}Ga-labeled AV01084 and AV01088 were calculated using $LogD_{7.4}$ measurement. The $LogD_{7.4}$ values of [^{68}Ga]Ga-AV01084 and [^{68}Ga]Ga-AV01088 were -3.61 ± 0.07 and -3.66 ± 0.25, respectively. The values indicate that both tracers are highly hydrophilic.

2.3. PET Imaging, ex vivo Biodistribution, and Blocking Studies

Representative PET images acquired at 1 h post-injection using [^{68}Ga]Ga-AV01084, [^{68}Ga]Ga-AV01088, [^{68}Ga]Ga-PSMA-617 and [^{68}Ga]Ga-AV02070 are provided in Figure 3. All the radiotracers were excreted primarily through the renal pathway. LNCaP tumor xenografts were clearly visualized by [^{68}Ga]Ga-AV01084 and [^{68}Ga]Ga-AV01088, but not visualized by [^{68}Ga]Ga-AV02070 (Figure 3A). HEK293T:hFAP tumor xenografts were barely visualized by the bispecific tracers ([^{68}Ga]Ga-AV01084 and [^{68}Ga]Ga-AV01088), but not visualized by [^{68}Ga]Ga-PSMA-617 (Figure 3B). The bispecific tracers have bone and joint uptake, which is commonly observed for FAP-targeted tracers. There was a high kidney uptake in mice injected with the bispecific tracers and [^{68}Ga]Ga-PSMA-617, but not in mice injected with [^{68}Ga]Ga-AV02070. Co-injection of [^{68}Ga]Ga-AV01088 with the PSMA inhibitor 2-PMPA (500 μg) reduced the uptake of [^{68}Ga]Ga-AV01088 in LNCaP tumors to almost background level (Figure 3A), confirming the uptake is PSMA-mediated. Similarly, co-injection of [^{68}Ga]Ga-AV01088 with FAPI-04 (250 μg) reduced the uptake of [^{68}Ga]Ga-AV01088 in HEK293T:hFAP tumors to almost background level (Figure 3B), confirming the uptake is FAP-mediated.

Preprints (www.preprints.org) | NOT PEER-REVIEWED | Posted: 13 November 2023 doi:10.20944/preprints202311.0769.v1

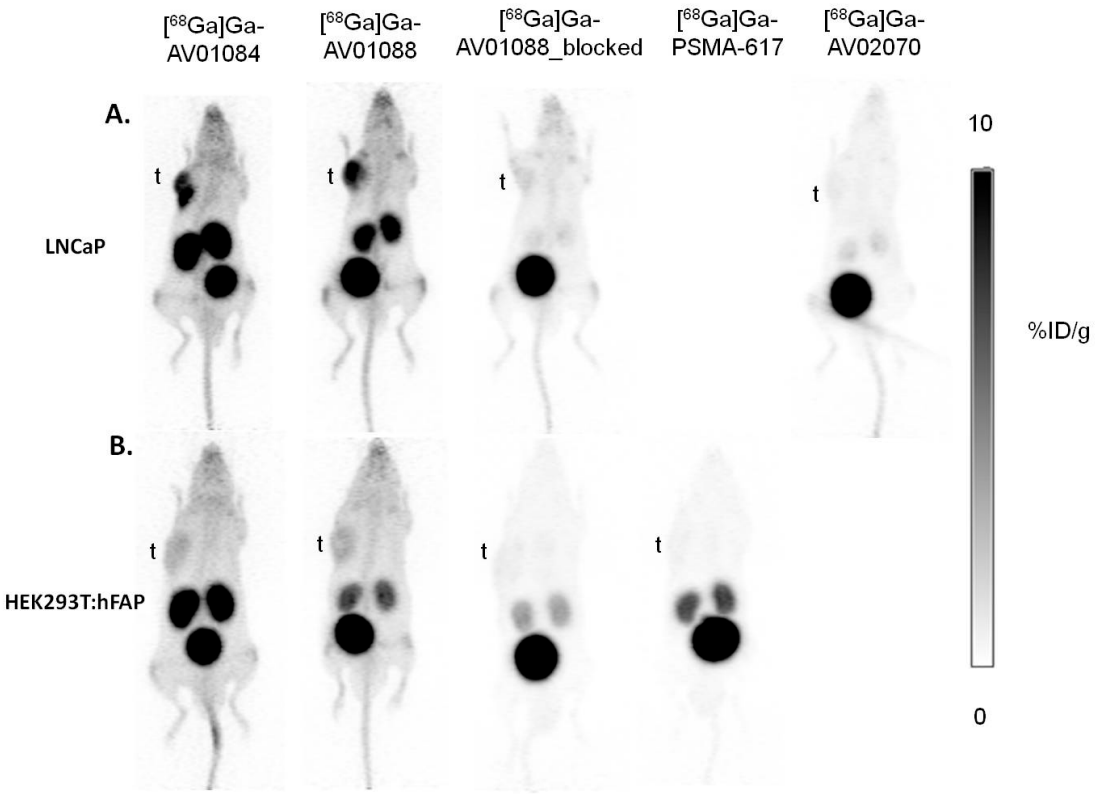

Figure 3. Representative maximum-intensity-projection PET images of [68Ga]Ga-AV01084, [68Ga]Ga-AV01088, [68Ga]Ga-PSMA-617, and [68Ga]Ga-AV02070 acquired at 1 h post-injection in mice bearing (A) LNCaP tumor xenografts and (B) HEK293T:hFAP tumor xenografts. The blocking with 2-PMPA (in LNCaP tumor xenografts) and FAPI-04 (in HEK293T:hFAP tumor xenografts) decreased the tumor uptake to background level. t: tumor.

Biodistribution studies were conducted at 1 h post-injection with 68Ga-labeled AV01084, AV01088, and AV02070 in LNCaP tumor-bearing mice (Figure 4, Table S4), and the previously reported data from [68Ga]Ga-PSMA-617 obtained using the same tumor model are included for comparison [33]. The results were consistent with the observation from their PET images. Tumor uptake values of [68Ga]Ga-AV01084, [68Ga]Ga-AV01088, [68Ga]Ga-PSMA-617 and [68Ga]Ga-AV02070 were 9.05 ± 1.54, 8.85 ± 1.25, 16.7 ± 2.30, and 0.74 ± 0.21 %ID/g, respectively. There was a very low tumor uptake in mice injected with [68Ga]Ga-AV02070, showing a very minimal FAP expression level in this tumor model. The uptake levels of these tracers in major organs and tissues are consistent with the trends observed in their PET images of LNCaP tumor-bearing mice. The bispecific tracers ([68Ga]Ga-AV01084 and [68Ga]Ga-AV01088) have significantly higher blood and bone uptake values than the monospecific tracers, [68Ga]Ga-PSMA-617 and [68Ga]Ga-AV02070 (blood uptake: 1.56-2.26 vs 0.28-0.75 %ID/g, $p < 0.05$; bone uptake: 0.88-2.47 vs 0.09-0.56 %ID/g, $P < 0.05$). This results in significantly lower tumor-to-blood ratio (4.09 ± 0.77 for [68Ga]Ga-AV01084, 4.10 ± 0.88 for [68Ga]Ga-AV01088 and 27.7 ± 6.28 for [68Ga]Ga-PSMA-617) and lower tumor-to-bone ratio (3.70 ± 0.83 for [68Ga]Ga-AV01084, 3.75 ± 1.28 for [68Ga]Ga-AV01088, and 96.5 ± 47.6 for [68Ga]Ga-PSMA-617). [68Ga]Ga-AV01084 has higher heart, kidney and adrenal glands uptake than [68Ga]Ga-AV01088 (Figure 4, $P < 0.05$).

Preprints (www.preprints.org) | NOT PEER-REVIEWED | Posted: 13 November 2023 doi:10.20944/preprints202311.0769.v1

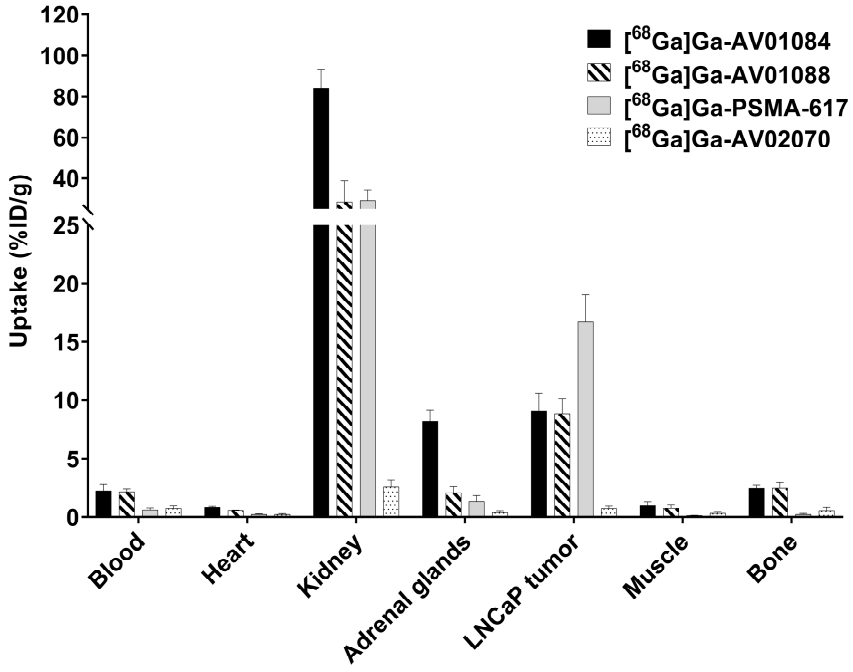

Figure 4. Biodistribution of [^{68}Ga]Ga-AV01084, [^{68}Ga]Ga-AV01088, [^{68}Ga]Ga-PSMA-617 and [^{68}Ga]Ga-AV02070 in LNCaP tumor-bearing mice. Error bars indicate standard deviation. The data of [^{68}Ga]Ga-PSMA-617 have been reported previously [33], and are included here for comparison.

Biodistribution studies were also conducted at 1 h post-injection with [^{68}Ga]Ga-AV01084, [^{68}Ga]Ga-AV01088 and [^{68}Ga]Ga-PSMA-617 in HEK293T:hFAP tumor-bearing mice (Figure 5 and Table S5), and the previously reported data from [^{68}Ga]Ga-AV02070 [31] using the same tumor model are included for comparison. Tumor uptake values of [^{68}Ga]Ga-AV01084, [^{68}Ga]Ga-AV01088, [^{68}Ga]Ga-PSMA-617 and [^{68}Ga]Ga-AV02070 were 1.90 ± 0.41, 1.20 ± 0.25, 0.26 ± 0.01, and 7.93 ± 1.88 %ID/g, respectively. There was a very low tumor uptake in mice injected with [^{68}Ga]Ga-PSMA-617, showing very minimal PSMA expression in this tumor model. The uptake levels of these tracers in the major organs and tissues are consistent with the trends observed in their PET images of HEK293T:hFAP tumor-bearing mice (Figure 4B and Table S5)

Preprints (www.preprints.org) | NOT PEER-REVIEWED | Posted: 13 November 2023 doi:10.20944/preprints202311.0769.v1

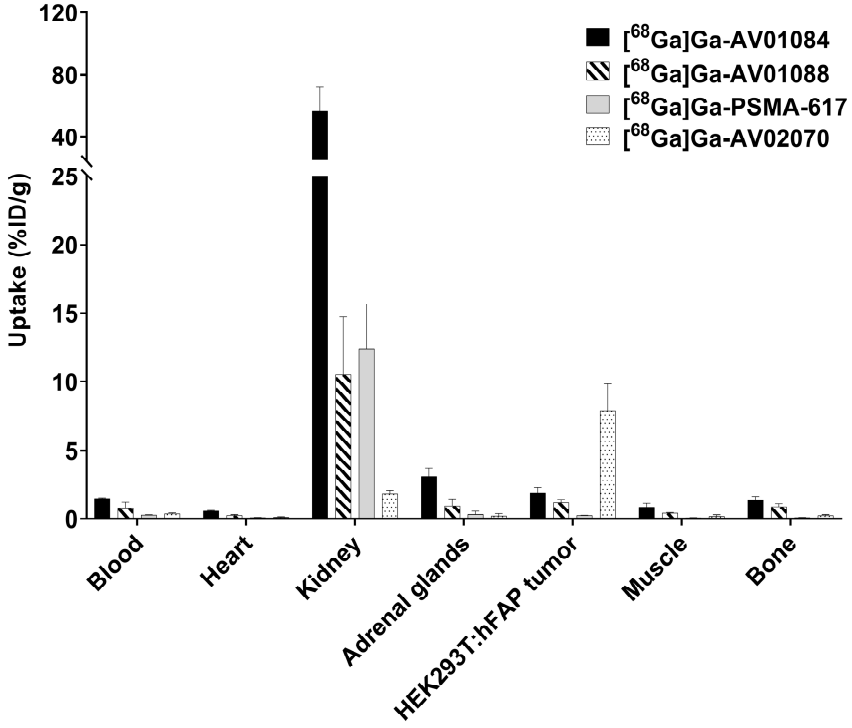

Figure 5. Biodistribution of [68Ga]Ga-AV01084, [68Ga]Ga-AV01088, [68Ga]Ga-PSMA-617 and [68Ga]Ga-AV02070 in HEK293T:hFAP tumor-bearing mice. Error bars indicate standard deviation. The data of [68Ga]Ga-AV02070 have been reported previously [31], and are included here for comparison.

Co-injection of 2-PMPA reduced the average uptake of [68Ga]Ga-AV01088 in LNCaP tumor xenografts by 67% (8.85 ± 1.25 %ID/g down to 2.95 ± 1.13 %ID/g at 1 h post-injection), confirming the specific uptake of [68Ga]Ga-AV01088 in LNCaP tumor xenografts (Figure 6). Co-injection of FAPI-04 reduced the average uptake of [68Ga]Ga-AV01088 in HEK293T:hFAP tumor xenografts by 43% (1.2 ± 0.25 %ID/g down to 0.51 ± 0.14 %ID/g at 1 h post-injection), confirming the specific uptake of [68Ga]Ga-AV01088 in HEK293T:hFAP tumor xenografts as well.

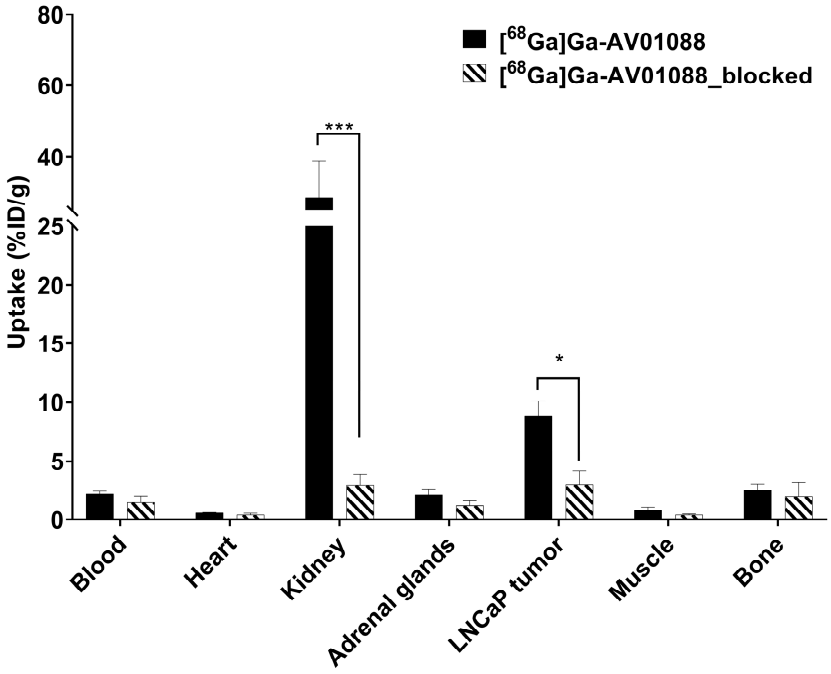

 doi:10.20944/preprints202311.0769.v1

Figure 6. Comparison of [^{68}Ga]Ga-AV01088 with and without co-injection of 2-PMPA on the uptake in LNCaP tumor xenografts and major organs/tissues in mice at 1 h post-injection. Error bars indicate standard deviation. *$p < 0.05$, ***$p < 0.001$.

3. Discussion

Previously, we synthesized three ^{68}Ga-labeled bispecific PSMA/FAP radiotracers, [^{68}Ga]Ga-AV01017, [^{68}Ga]Ga-AV01030, and [^{68}Ga]Ga-AV01038 [28], which incorporate a quinoline-based FAP-targeted pharmacophore and an anthracene-based PSMA-targeted pharmacophore of [^{68}Ga]Ga-HTK03041. The PSMA and FAP *in vitro* competition binding assays indicated that our bispecific tracers have lower binding affinity to PSMA compared to the monospecific PSMA-targeted ligand, Ga-HTK03041, but maintained a similar binding affinity to FAP when compared to the monospecific FAP-targeted ligand, Ga-FAPI-04. However, the bispecific tracers have higher uptake in major organs (blood, muscle, bone, and heart) and decreased tumor uptake in the mouse models in comparison to the ^{68}Ga-labeled monospecific counterparts, [^{68}Ga]Ga-HTK03041 and [^{68}Ga]Ga-FAPI-04.

Therefore, in this report we selected the pharmacophores of [^{68}Ga]Ga-PSMA-617 (in brown, Figure 1) and [^{68}Ga]Ga-AV02070 (in blue, Figure 1) for the design of our PSMA/FAP bispecific tracers as they are more hydrophilic and have high affinity for PSMA and FAP, respectively. These two pharmacophores are separated by a Lys-Gly linker (Figure 1B). The PSMA-targeted pharmacophore (Lys(tranexamic acid-2-Nal)-urea-Glu and the linker (Lys-Gly) was constructed directly on solid phase using the commercially available amino acids. For AV01084, the pyridine-based FAP-targeted ligand and the DOTA chelator were coupled to the α-amino group and side-chain of Lys, respectively. While for AV01088, the DOTA chelator and the pyridine-based FAP-targeted ligand were coupled to the α-amino group and side-chain of Lys, respectively. This allows us to investigate the effect of the position of the DOTA chelator on binding affinity and biodistribution of the bispecific tracers.

The enzymatic assay (Figure 2B) confirmed that the FAP binding affinities of Ga-AV01084 (IC_{50} = 10.9 ± 0.67 nM) and Ga-AV01088 (IC_{50} = 16.7 ± 1.53 nM) were comparable or even slightly better than that of the previously reported Ga-AV02070 (IC_{50} = 17.1 ± 4.60 nM) [31]. To investigate if the PSMA-targeted pharmacophore has any effect on the overall FAP binding of our bispecific ligands, we also measured the FAP binding affinity of Ga-PSMA-617. The very weak binding affinity of Ga-PSMA-617 (IC_{50} > 1,000 nM) suggests that the potent FAP binding affinity of our bispecific ligands is contributed mainly by the AV02070 pharmacophore.

The PSMA binding affinities of the bispecific ligands (K_i = 11.6 – 28.7 nM) were inferior to that of Ga-PSMA-617 (K_i = 1.23 ± 0.08) [33]. However, when compared to the bispecific tracers from our previous report (K_i = 20.1–54.4 nM), changing Ala(9-Anth) to 2-Nal, and changing quinoline to pyridine significantly increased the binding affinity of PSMA/FAP bispecific tracers to PSMA. This supports our hypothesis that there might be an interaction between the pharmacophores that interferes with the overall binding of the bispecific ligands to PSMA. Moreover, Ga-AV02070 has very minimal binding affinity to PSMA (K_i > 1,000 nM), indicating that the PSMA binding affinity of our bispecific ligands is contributed mainly by the PSMA-617 pharmacophore.

Despite having a lower uptake in the LNCaP tumor compared to [^{68}Ga]Ga-PSMA-617 (16.7 ± 2.30 %ID/g), [^{68}Ga]Ga-AV01084 and [^{68}Ga]Ga-AV01088 (9.05 ± 1.54 and 8.85 ± 1.25 %ID/g, respectively) had better tumor uptake than our previously reported three bispecific PSMA/FAP tracers ([^{68}Ga]Ga-AV01017, [^{68}Ga]Ga-AV01030 and [^{68}Ga]AV01038) (4.25 – 5.17 %ID/g) [28]. Moreover, co-injection of [^{68}Ga]Ga-AV01088 with 2-PMPA decreased the tumor uptake by 67%, indicating that the tumor uptake is specific to PSMA. We also observed a significant bone uptake (1.97 ± 1.15 %ID/g) when [^{68}Ga]Ga-AV01088 was co-injected with 2-PMPA, whereas there was a decreased bone uptake to background level (0.20 ± 0.06 %ID/g) when [^{68}Ga]Ga-AV01088 was co-injected with FAPI-04. This indicates that the bone uptake of [^{68}Ga]Ga-AV01088 might be due to specific binding of the FAP-targeted pharmacophore. Uptake of [^{68}Ga]Ga-AV01088 to HEK293T:hFAP tumor is also FAP-mediated, as demonstrated by the significantly decreased tumor uptake obtained when co-injected with FAPI-04.

 doi:10.20944/preprints202311.0769.v1

Unlike the improved uptake in LNCaP tumor xenografts, the uptake of [^{68}Ga]Ga-AV01084 and [^{68}Ga]Ga-AV01088 (1.20-1.90 %ID/g) in HEK293T:hFAP tumor xenografts remains significantly lower than that of the monospecific counterpart, [^{68}Ga]Ga-AV02070 (7.93 ± 1.88 %ID/g, $P < 0.05$). One possible reason is the addition of the succinic acid linker, which might have interfered with the binding of our tracers to FAP, thus decreasing the tumor uptake. Piperazine-based linkers have been shown to be important for maintaining good tumor uptake of FAP-targeted tracers [34]. Therefore, incorporating a piperazine-based linker can also be considered for future modifications to improve uptake of PSMA/FAP bispecific tracers to the FAP-expressing tumors.

Compared to the monospecific tracers, the bispecific tracers have higher blood, bone, and muscle uptake. However, the current modified tracers have significantly decreased blood retention (0.79 – 2.26 %ID/g) when compared to the PSMA/FAP bispecific tracers in our previous report (5.75 – 11.94 %ID/g) [28]. This leads to better LNCaP tumor-to-blood contrast ratios for [^{68}Ga]Ga-AV01084 (4.09 ± 0.77) and [^{68}Ga]Ga-AV01088 (4.10 ± 0.88) (Table S4) than our previously reported PSMA/FAP bispecific tracers (0.48 – 0.89) [28]. The decreased blood retention might be contributed by increased hydrophilicity of the new bispecific tracers shown by their low $LogD_{7.4}$ values (< –3.60). This is consistent with previous findings that more hydrophilic radiotracers will have faster pharmacokinetics and clearance, hence, have better tumor-to-background contrast ratio [35]. In addition, there are no significant differences in the tumor uptake or the tumor-to-background contrast ratios between [^{68}Ga]Ga-AV01084 and [^{68}Ga]Ga-AV01088, which indicates that the position of the DOTA chelator to the lysine linker does not have a crucial effect on the pharmacokinetics of the tracers.

Previously, Wang et al. [27] reported a ^{68}Ga-labeled PSMA/FAP bispecific tracer, [^{68}Ga]Ga-FAPI-PSMA (Figure 7), consisting of a PSMA-targeted pharmacophore from PSMA-617 (in brown, Figure 7) and an FAP-targeted pharmacophore from FAPI-04 (in blue). It would be difficult to directly compare the performance of our bispecific radiotracers with [^{68}Ga]Ga-FAPI-PSMA as different tumor models were used for evaluation: PSMA-expressing LNCaP tumors and FAP-expressing HEK293T:hFAP tumors used in this report; PSMA-expressing 22Rv1 tumors and FAP-expressing U87 MG tumors used by Wang et al [27]. [^{68}Ga]Ga-FAPI-PSMA was shown to have better tumor uptake (SUVmax = 1.32 and 1.67 for 22Rv1 and U87 MG tumors, respectively) compared to the monospecific tracers, [^{68}Ga]Ga-PSMA-617 (SUVmax = 0.25 for 22Rv1 tumors) and [^{68}Ga]Ga-FAPI-04 (SUVmax = 0.45 for U87 MG tumors). This demonstrates the potential of utilizing PSMA/FAP bispecific tracers to improve the tumor uptake. However, similar to our results, [^{68}Ga]Ga-FAPI-PSMA also had higher background uptake compared to the monospecific tracers.

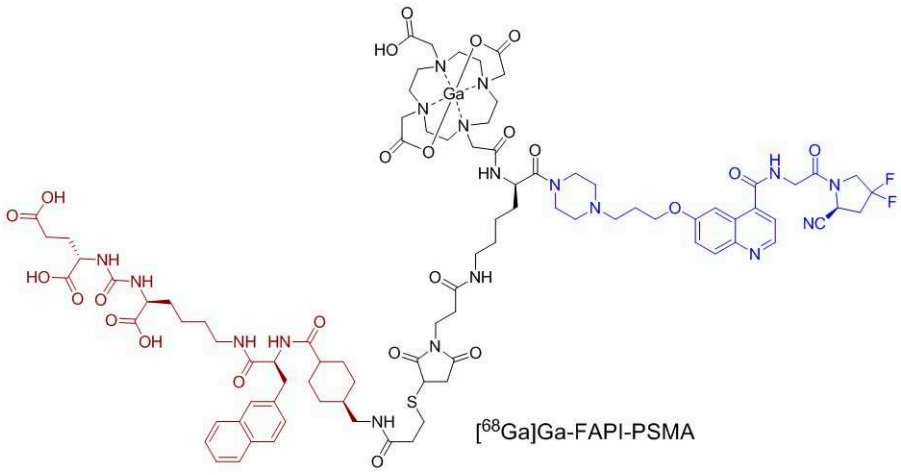

Figure 7. The chemical structure of [^{68}Ga]Ga-FAPI-PSMA [27]. The PSMA- and FAP- targeted pharmacophores are shown in brown and blue, respectively.

Replacing the quinoline-based FAP-targeted pharmacophore with a pyridine-based FAP-targeted pharmacophore helps decrease the background uptake (blood, bone, and muscle) of the

 doi:10.20944/preprints202311.0769.v1

bispecific tracers, however it also results in a significantly lower uptake in HEK293T:hFAP tumors. Therefore, future attempts on the use of a pyridine-based FAP-targeted pharmacophore for the design of PSMA/FAP bispecific tracers need to include optimization of linkers such as the use of a piperazine-based linker to further improve FAP binding affinity and tumor uptake.

4. Materials and Methods

4.1. Synthesis of Bispecific PSMA/FAP-targeted Ligands

Detailed information for the synthesis, purification, and characterizations of AV01084 and AV01088, and their nonradioactive Ga-complexed standards and ^{68}Ga-labeled analogs are provided in the Supplementary Materials (Tables S1-S3).

4.2. Cell Culture

The LNCaP cells obtained from ATCC (via Cedarlane, Burlington, Canada) were cultured in RPMI 1640 medium supplemented with 10% FBS, penicillin (100 U/mL) and streptomycin (100 µg/mL) at 37 °C in a Panasonic Healthcare (Tokyo, Japan) MCO-19AIC humidified incubator containing 5% CO_2. The HEK293T:hFAP cells [28] were cultured in DMEM GlutaMAX™ medium supplemented with 10% FBS, penicillin (100 U/mL) and streptomycin (100 µg/mL). Cells were grown until 80-90% confluence and washed with sterile phosphate-buffered saline (PBS, pH 7.4) and collected after 1 min trypsinization. The cell concentration was counted in triplicate using a hemocytometer and a manual laboratory counter.

4.3. LogD$_{7.4}$ Measurement

The lipophilicity characteristics of the ^{68}Ga-labeled tracers were determined by calculating the logarithm of the distribution coefficient (logD) in n-octanol/phosphate-buffered solution (PBS) of pH 7.40. Purified ^{68}Ga-labeled tracer (50 µL) was added into a test tube containing 3 mL n-octanol and 3 mL PBS. The mixture was vortexed for 1 min, followed by centrifugation for 15 min at 3,000 rpm. The two layers (1 mL each) were then collected separately and the radioactivity was counted using a Perkin Elmer (Waltham, MA, USA) Wizard2 2480 automatic gamma counter. After adjusting the counts to background and calculating the ratio of the activity of the organic to that of the aqueous phase, the logD$_{7.4}$ values were calculated.

4.4. In vitro PSMA Competition Binding Assay

The PSMA binding assays were conducted following previously published procedures using LNCaP cells and [^{18}F]DCFPyL as the radioligand [28,33,36]. Data analyses of K_i were performed using the nonlinear regression algorithm of GraphPad Prism 7 (San Diego, CA) software.

4.5. In vitro FAP Fluorescence Assay

The half-maximal inhibitory concentration (IC_{50}) values of the tested ligands for FAP were measured by *in vitro* enzymatic assay following previously published procedures [28,31]. The recombinant human FAP (Biolegend; 0.2 µg/mL, 50 µL) was added into costar 96-well plate. PBS and varied concentrations (0.2 pM to 2 µM) of tested nonradioactive Ga-complexed standards were added to each wells (in duplicate) containing the recombinant human FAP. After being incubated for 30 min at 37 °C, 50 µL of Suc-Gly-Pro-AMC (2 µM, Bachem) was added to each well. The fluorescent signals were acquired at 15, 30, 45, and 60 min using FlexStation 3 Multi-Mode Microplate Reader with excitation at 380 nm and emission at 460 nm. The IC_{50}(FAP) was calculated using "nonlinear fit model" built-in model in GraphPad Prism 7.02 software.

4.6. Ex vivo Biodistribution and PET/CT Imaging Studies

Imaging and biodistribution studies were performed using male NOD.Cg-Rag1tm1Mom Il2rgtm1Wjl/SzJ (NRG) mice following previously published procedures [37–39]. The experiments

were conducted according to the guidelines established by the Canadian Council on Animal Care and approved by Animal Ethics Committee of the University of British Columbia. The mice were briefly sedated by inhalation of 2.5% isoflurane in oxygen, and 100 μL LNCaP (2×10^5 cells) or HEK293T:hFAP (8.5×10^6 cells) cells were inoculated subcutaneously behind the left shoulder. When the tumor grew to 5 – 8 mm in diameter over 3 – 4 weeks and 4 – 5 weeks for HEK293T:hFAP and LNCaP tumors, respectively, the mice were used for PET/CT imaging and biodistribution studies.

PET/CT imaging experiments were carried out using a Siemens (Knoxville, TN, USA) Inveon micro PET/CT scanner. Each tumor-bearing mouse was injected with ~4 – 6 MBq of ^{68}Ga-labeled tracer through a lateral caudal tail vein under 2.5% isoflurane in oxygen anesthesia, followed by recovery and roaming freely in its cage during the uptake period. At 50 min post-injection, a 10-min CT scan was conducted first for localization and attenuation correction after segmentation for reconstructing the PET images, followed by a 10-min static PET imaging acquisition.

For biodistribution studies, the mice were injected with the radiotracer (~2 – 4 MBq) as described above. For blocking studies, PSMA tumor-bearing mice were co-injected with 2-PMPA (500 μg/mouse) and HEK293T:hFAP tumor-bearing mice were co-injected with FAPI-04 (250 μg/mouse). At 1 h post-injection, the mice were euthanized by CO_2 inhalation. Blood was withdrawn by cardiac puncture, and organs/tissues of interest were collected, weighed and counted using a Perkin Elmer Wizard2 2480 automatic gamma counter.

4.7. Statistical Analysis

Data were analyzed with the GraphPad Prism, version 7.02 and Microsoft (Redmond, WA, USA) Excel software. One way ANOVA and multiple *t* tests were performed for all organs in the biodistribution studies of [^{68}Ga]Ga-AV01084 and [^{68}Ga]Ga-AV01088 in LNCaP and HEK293T:hFAP tumor models. A statistically significant difference was considered present when the adjusted *P* value was less than 0.05 using the Holm–Sidak method.

5. Conclusions

Two novel ^{68}Ga-labeled PSMA/FAP bispecific tracers were designed, synthesized, and confirmed to have the ability to bind both PSMA and FAP *in vitro* and *in vivo*. Compared with the monospecific tracers, the bispecific tracers have decreased binding affinities towards PSMA, but retain comparable binding affinities towards FAP. Compared with three of our previously reported PSMA/FAP bispecific tracers ([^{68}Ga]Ga-AV01017, [^{68}Ga]Ga-AV01030, and [^{68}Ga]Ga-AV01038), both [^{68}Ga]Ga-AV01084 and Ga-AV01088 have better PSMA binding affinity, and improved tumor uptake in PSMA-expressing xenografts and tumor-to-background (blood, muscle, and bone) contrast ratios. Further optimization on the selection of linkers should be explored to improve the binding affinity, pharmacokinetics, and tumor uptake of the PSMA/FAP bispecific tracers.

Supplementary Materials: The following supporting information can be downloaded at the website of this paper posted on Preprints.org. Detailed synthetic procedures and results for the preparation of PSMA/FAP bispecific ligands, and their ^{nat}Ga/^{68}Ga-complexed analogs [29,31,33,40,41]; Table S1: HPLC purification conditions and MS characterizations of DOTA-conjugated precursors; Table S2: HPLC purification conditions and MS characterizations of nonradioactive Ga-complexed standards; Table S3: HPLC conditions for the purification and quality control of ^{68}Ga-labeled tracers; Table S4: Biodistribution and uptake ratios of ^{68}Ga-labeled PSMA/FAP bispecific tracers, PSMA-617 and AV02070 in LNCaP tumor-bearing mice; Table S5: Biodistribution and uptake ratios of ^{68}Ga-labeled PSMA/FAP bispecific tracers, PSMA-617 and AV02070 in HEK293T:hFAP tumor-bearing mice.

Author Contributions: Conceptualization, K.-S.L. and A.V.; methodology, A.V., H.M., C.-C.C., D.E.C., S.B., L.W. and A.A.W.L.W.; validation, A.V., C.-C.C., D.E.C., S.B., L.W. and K.-S.L.; formal analysis, A.V., C.-C.C., D.E.C., S.B., L.W. and A.A.W.L.W.; investigation, A.V., C.-C.C., D.E.C., S.B. and L.W.; resources, H.M., F.B. and K.-S.L.; data curation, A.V., A.A.W.L.W. and K.-S.L.; writing—original draft preparation, A.V. and A.A.W.L.W.; writing—review and editing, K.-S.L.; visualization, A.V.; supervision, H.M., K.-S.L. and F.B.; project administration, H.M. and K.-S.L.; funding acquisition, F.B. and K-S.L. All authors have read and agreed to the published version of the manuscript.

Funding: This research was supported by the Canadian Institutes of Health Research (PJT-162243, PJT-180299 and PJT-180300).

Institutional Review Board Statement: The animal study protocol (A20-0113) was approved by the Animal Ethics Committee of the University of British Columbia on 30 September 2020

Informed Consent Statement: Not applicable

Data Availability Statement: The data presented in this study are available in the Supplementary Materials

Acknowledgments: We thank Jinhe Pan for his help in the production of [^{18}F]DCFPyL for use in the PSMA binding assays, and Nadine Colpo and Pauline Ng for their help in the animal studies.

Conflicts of Interest: François Bénard and Kuo-Shyan Lin are co-founders and consultants of Alpha-9 Theranostics Inc., and receive research funding from the company. François Bénard, Kuo-Shyan Lin and Helen Merkens hold shares and/or options in Alpha-9. The funder had no role in the design of the study; in the collection, analyses, or interpretation of data; in the writing of the manuscript; or in the decision to publish the results.

References

1. Sung, H.; Ferlay, J.; Siegel, R. L.; Laversanne, M.; Soerjomataram, I.; Jemal, A.; Bray, F. Global Cancer Statistics 2020: GLOBOCAN Estimates of Incidence and Mortality Worldwide for 36 Cancers in 185 Countries. *CA. Cancer J. Clin.* **2021**, *71*, 209–249.
2. Siegel, R. L.; Miller, K. D.; Wagle, N. S.; Jemal, A. Cancer Statistics, 2023. *CA. Cancer J. Clin.* **2023**, *73*, 17–48.
3. Sartor, O.; de Bono, J.; Chi, K. N.; Fizazi, K.; Herrmann, K.; Rahbar, K.; Tagawa, S. T.; Nordquist, L. T.; Vaishampayan, N.; El-Haddad, G.; et al. Lutetium-177–PSMA-617 for Metastatic Castration-resistant Prostate Cancer. *N. Engl. J. Med.* **2021**, *385*, 1091–1103..
4. Fassbind, S.; Ferraro, D. A.; Stelmes, J.-J.; Fankhauser, C. D.; Guckenberger, M.; Kaufmann, P. A.; Eberli, D.; Burger, I. A.; Kranzbühler, B. ^{68}Ga-PSMA-11 PET Imaging in Patients with Ongoing Androgen Deprivation Therapy for Advanced Prostate Cancer. *Ann. Nucl. Med.* **2021**, *35*, 1109–1116.
5. Carlucci, G.; Ippisch, R.; Slavik, R.; Mishoe, A.; Blecha, J.; Zhu, S. ^{68}Ga-PSMA-11 NDA Approval: A Novel and Successful Academic Partnership. *J. Nucl. Med.* **2021**, *62*, 149–155.
6. Strauss, D. S.; Sachpekidis, C.; Kopka, K.; Pan, L.; Haberkorn, U.; Dimitrakopoulou-Strauss, A. Pharmacokinetic Studies of [^{68}Ga]Ga-PSMA-11 in Patients with Biochemical Recurrence of Prostate Cancer: Detection, Differences in Temporal Distribution and Kinetic Modelling by Tissue Type. *Eur. J. Nucl. Med. Mol. Imaging* **2021**, 48, 4472–4482.
7. Kaittanis, C.; Andreou, C.; Hieronymus, H.; Mao, N.; Foss, C. A.; Eiber, M.; Weirich, G.; Panchal, P.; Gopalan, A.; Zurita, J.; et al. Prostate-specific Membrane Antigen Cleavage of Vitamin B9 Stimulates Oncogenic Signaling through Metabotropic Glutamate Receptors. *J. Exp. Med.* **2017**, *215*, 159–175.
8. Rajasekaran, A. K.; Anilkumar, G.; Christiansen, J. J. Is Prostate-specific Membrane Antigen a Multifunctional Protein? *Am. J. Physiol. Cell Physiol.* **2005**, *288*, C975–C981.
9. Spatz, S.; Tolkach, Y.; Jung, K.; Stephan, C.; Busch, J.; Ralla, B.; Rabien, A.; Feldmann, G.; Brossart, P.; Bundschuh, R. A.; et al. Comprehensive Evaluation of Prostate Specific Membrane Antigen Expression in the Vasculature of Renal Tumors: Implications for Imaging Studies and Prognostic Role. *J. Urol.* **2018**, *199*, 370–377.
10. Wernicke, A. G.; Varma, S.; Greenwood, E. A.; Christos, P. J.; Chao, K. S. C.; Liu, H.; Bander, N. H.; Shin, S. J. Prostate-specific Membrane Antigen Expression in Tumor-associated Vasculature of Breast Cancers. *APMIS* **2014**, *122*, 482–489.
11. Haffner, M. C.; Laimer, J.; Chaux, A.; Schäfer, G.; Obrist, P.; Brunner, A.; Kronberger, I. E.; Laimer, K.; Gurel, B.; Koller, J.-B.; et al. High Expression of Prostate-specific Membrane Antigen in the Tumor-associated Neo-vasculature Is Associated with Worse Prognosis in Squamous Cell Carcinoma of the Oral Cavity. *Mod. Pathol.* **2012**, *25*, 1079–1085.
12. Paschalis, A.; Sheehan, B.; Riisnaes, R.; Rodrigues, D. N.; Gurel, B.; Bertan, C.; Ferreira, A.; Lambros, M. B. K.; Seed, G.; Yuan, W.; et al. Prostate-specific Membrane Antigen Heterogeneity and DNA Repair Defects in Prostate Cancer. *Eur. Urol.* **2019**, *76*, 469–478.
13. Isik, E. G.; Has-Simsek, D.; Sanli, O.; Sanli, Y.; Kuyumcu, S. Fibroblast Activation Protein–Targeted PET Imaging of Metastatic Castration-resistant Prostate Cancer Compared With ^{68}Ga-PSMA and ^{18}F-FDG PET/CT. *Clin. Nucl. Med.* **2022**, *47*, e54.
14. Seifert, R.; Seitzer, K.; Herrmann, K.; Kessel, K.; Schäfers, M.; Kleesiek, J.; Weckesser, M.; Boegemann, M.; Rahbar, K. Analysis of PSMA Expression and Outcome in Patients with Advanced Prostate Cancer Receiving ^{177}Lu-PSMA-617 Radioligand Therapy. *Theranostics* **2020**, *10*, 7812–7820.

15. Mannweiler, S.; Amersdorfer, P.; Trajanoski, S.; Terrett, J. A.; King, D.; Mehes, G. Heterogeneity of Prostate-specific Membrane Antigen (PSMA) Expression in Prostate Carcinoma with Distant Metastasis. *Pathol. Oncol. Res.* **2009**, *15*, 167–172.
16. Park, J. E.; Lenter, M. C.; Zimmermann, R. N.; Garin-Chesa, P.; Old, L. J.; Rettig, W. J. Fibroblast Activation Protein, a Dual Specificity Serine Protease Expressed in Reactive Human Tumor Stromal Fibroblasts. *J. Biol. Chem.* **1999**, *274*, 36505–36512.
17. Teichgräber, V.; Monasterio, C.; Chaitanya, K.; Boger, R.; Gordon, K.; Dieterle, T.; Jäger, D.; Bauer, S. Specific Inhibition of Fibroblast Activation Protein (FAP)-Alpha Prevents Tumor Progression in Vitro. *Adv. Med. Sci.* **2015**, *60*, 264–272.
18. Kesch, C.; Yirga, L.; Dendl, K.; Handke, A.; Darr, C.; Krafft, U.; Radtke, J. P.; Tschirdewahn, S.; Szarvas, T.; Fazli, L.; et al. High Fibroblast-activation-protein Expression in Castration-resistant Prostate Cancer Supports the Use of FAPI-molecular Theranostics. *Eur. J. Nucl. Med. Mol. Imaging* **2021**, *49*, 385–389.
19. Julia, T.; Zhang Paul, J.; Yingtao, B.; Celine, S.; Rajrupa, M.; Stephen, T.; Lo, A.; Haiying, C.; Carolyn, M.; June, C. H.; et al. Fibroblast Activation Protein Expression by Stromal Cells and Tumor-associated Macrophages in Human Breast Cancer. *Hum. Pathol.* **2013**, *44*, 2549–2557.
20. Henry, L. R.; Lee, H.-O.; Lee, J. S.; Klein-Szanto, A.; Watts, P.; Ross, E. A.; Chen, W.-T.; Cheng, J. D. Clinical Implications of Fibroblast Activation Protein in Patients with Colon Cancer. *Clin. Cancer Res.* **2007**, *13*, 1736–1741.
21. Kratochwil, C.; Flechsig, P.; Lindner, T.; Abderrahim, L.; Altmann, A.; Mier, W.; Adeberg, S.; Rathke, H.; Röhrich, M.; Winter, H.; et al. ^{68}Ga-FAPI PET/CT: Tracer Uptake in 28 Different Kinds of Cancer. *J. Nucl. Med.* **2019**, *60*, 801–805.
22. Wegen, S.; Roth, K. S.; Weindler, J.; Claus, K.; Linde, P.; Trommer, M.; Akuamoa-Boateng, D.; van Heek, L.; Baues, C.; Schömig-Markiefka, B.; et al. First Clinical Experience With [^{68}Ga]Ga-FAPI-46-PET/CT Versus [^{18}F]F-FDG PET/CT for Nodal Staging in Cervical Cancer. *Clin. Nucl. Med.*, **2023**, *48*, 150.
23. Baum, R. P.; Schuchardt, C.; Singh, A.; Chantadisai, M.; Robiller, F. C.; Zhang, J.; Mueller, D.; Eismant, A.; Almaguel, F.; Zboralski, D.; et al. Feasibility, Biodistribution, and Preliminary Dosimetry in Peptide-targeted Radionuclide Therapy of Diverse Adenocarcinomas Using ^{177}Lu-FAP-2286: First-in-humans Results. *J. Nucl. Med.* **2022**, *63*, 415–423.
24. Mendoza-Figueroa, M. J.; Escudero-Castellanos, A.; Ramirez-Nava, G. J.; Ocampo-García, B. E.; Santos-Cuevas, C. L.; Ferro-Flores, G.; Pedraza-Lopez, M.; Avila-Rodriguez, M. A. Preparation and Preclinical Evaluation of ^{68}Ga-iPSMA-BN as a Potential Heterodimeric Radiotracer for PET-imaging of Prostate Cancer. *J. Radioanal. Nucl. Chem.* **2018**, *318*, 2097–2105.
25. Boinapally, S.; Lisok, A.; Lofland, G.; Minn, I.; Yan, Y.; Jiang, Z.; Shin, M. J.; Merino, V. F.; Zheng, L.; Brayton, C.; et al. Hetero-bivalent Agents Targeting FAP and PSMA. *Eur. J. Nucl. Med. Mol. Imaging* **2022**, *49*, 4369–4381.
26. Hu, K.; Li, L.; Huang, Y.; Ye, S.; Zhong, J.; Yan, Q.; Zhong, Y.; Fu, L.; Feng, P.; Li, H. Radiosynthesis and Preclinical Evaluation of Bispecific PSMA/FAP Heterodimers for Tumor Imaging. *Pharmaceuticals* **2022**, *15*, 383.
27. Wang, P.; Wang, S.; Liu, F.; Ren, Y.; Guo, Q.; Zhang, Q.; Hou, X.; Yao, Y.; Zhu, H.; Yang, Z. Preclinical Evaluation of a Fibroblast Activation Protein and a Prostate-specific Membrane Antigen Dual-targeted Probe for Noninvasive Prostate Cancer Imaging. *Mol. Pharmaceutics* **2023**, *20*, 1415–1425.
28. Verena, A.; Zhang, Z.; Kuo, H.-T.; Merkens, H.; Zeisler, J.; Wilson, R.; Bendre, S.; Wong, A. A. W. L.; Bénard, F.; Lin, K.-S. Synthesis and Preclinical Evaluation of Three Novel ^{68}Ga-labeled Bispecific PSMA/FAP-targeting Tracers for Prostate Cancer Imaging. *Molecules* **2023**, *28*, 1088.
29. Jansen, K.; Heirbaut, L.; Verkerk, R.; Cheng, J. D.; Joossens, J.; Cos, P.; Maes, L.; Lambeir, A.-M.; De Meester, I.; Augustyns, K.; et al. Extended Structure–activity Relationship and Pharmacokinetic Investigation of (4-Quinolinoyl)glycyl-2-cyanopyrrolidine Inhibitors of Fibroblast Activation Protein (FAP). *J. Med. Chem.* **2014**, *57*, 3053–3074.
30. Poplawski, S. E.; Lai, J. H.; Li, Y.; Jin, Z.; Liu, Y.; Wu, W.; Wu, Y.; Zhou, Y.; Sudmeier, J. L.; Sanford, D. G.; et al. Identification of Selective and Potent Inhibitors of Fibroblast Activation Protein and Prolyl Oligopeptidase. *J. Med. Chem.* **2013**, *56*, 3467–3477.
31. Verena, A.; Kuo, H.-T.; Merkens, H.; Zeisler, J.; Bendre, S.; Wong, A. A. W. L.; Bénard, F.; Lin, K.-S. Novel ^{68}Ga-Labeled Pyridine-based Fibroblast Activation Protein-targeted Tracers with High Tumor-to-background Contrast. *Pharmaceuticals* **2023**, *16*, 449.
32. Benešová, M.; Schäfer, M.; Bauder-Wüst, U.; Afshar-Oromieh, A.; Kratochwil, C.; Mier, W.; Haberkorn, U.; Kopka, K.; Eder, M. Preclinical Evaluation of a Tailor-made DOTA-conjugated PSMA Inhibitor with Optimized Linker Moiety for Imaging and Endoradiotherapy of Prostate Cancer. *J. Nucl. Med.* **2015**, *56*, 914–920.
33. Kuo, H.-T.; Pan, J.; Zhang, Z.; Lau, J.; Merkens, H.; Zhang, C.; Colpo, N.; Lin, K.-S.; Bénard, F. Effects of Linker Modification on Tumor-to-kidney Contrast of ^{68}Ga-labeled PSMA-targeted Imaging Probes. *Mol. Pharmaceutics* **2018**, *15*, 3502–3511.

34. Imlimthan, S.; Moon, E. S.; Rathke, H.; Afshar-Oromieh, A.; Rösch, F.; Rominger, A.; Gourni, E. New Frontiers in Cancer Imaging and Therapy Based on Radiolabeled Fibroblast Activation Protein Inhibitors: A Rational Review and Current Progress. *Pharmaceuticals* **2021**, *14*, 1023.
35. Nguyen, A. T.; Kim, H.-K. Recent Developments in PET and SPECT Radiotracers as Radiopharmaceuticals for Hypoxia Tumors. *Pharmaceutics* **2023**, *15*, 1840.
36. Kuo, H.-T.; Lin, K.-S.; Zhang, Z.; Uribe, C. F.; Merkens, H.; Zhang, C.; Bénard, F. ^{177}Lu-Labeled Albumin-binder-conjugated PSMA-targeting Agents with Extremely High Tumor Uptake and Enhanced Tumor-to-kidney Absorbed Dose Ratio. *J. Nucl. Med.* **2021**, *62*, 521–527.
37. Bratanovic, I. J.; Zhang, C.; Zhang, Z.; Kuo, H.-T.; Colpo, N.; Zeisler, J.; Merkens, H.; Uribe, C.; Lin, K.-S.; Bénard, F. A Radiotracer for Molecular Imaging and Therapy of Gastrin-releasing Peptide Receptor-Positive Prostate Cancer. *J. Nucl. Med.* **2022**, *63*, 424–430.
38. Lau, J.; Rousseau, E.; Zhang, Z.; Uribe, C. F.; Kuo, H.-T.; Zeisler, J.; Zhang, C.; Kwon, D.; Lin, K.-S.; Bénard, F. Positron Emission Tomography Imaging of the Gastrin-releasing Peptide Receptor with a Novel Bombesin Analogue. *ACS Omega* **2019**, *4*, 1470–1478.
39. Lin, K.-S.; Pan, J.; Amouroux, G.; Turashvili, G.; Mesak, F.; Hundal-Jabal, N.; Pourghiasian, M.; Lau, J.; Jenni, S.; Aparicio, S.; et al. In Vivo Radioimaging of Bradykinin Receptor B1, a Widely Overexpressed Molecule in Human Cancer. *Cancer Res.* **2015**, *75*, 387–393.
40. Wünsch, M.; Schröder, D.; Fröhr, T.; Teichmann, L.; Hedwig, S.; Janson, N.; Belu, C.; Simon, J.; Heidemeyer, S.; Holtkamp, P.; et al. Asymmetric Synthesis of Propargylamines as Amino Acid Surrogates in Peptidomimetics. *Beilstein J. Org. Chem.* **2017**, *13*, 2428–2441.
41. Benešová, M.; Bauder-Wüst, U.; Schäfer, M.; Klika, K. D.; Mier, W.; Haberkorn, U.; Kopka, K.; Eder, M. Linker Modification Strategies to Control the Prostate-specific Membrane Antigen (PSMA)-targeting and Pharmacokinetic Properties of DOTA-conjugated PSMA Inhibitors. *J. Med. Chem.* **2016**, *59*, 1761–1775.